NIPER/BDM-0329

Topical Report

THREE-PHASE RELATIVE PERMEABILITY CHARACTERISTICS OF A DOLOMITE ROCK PLUG

for

Management and Operating Contract for the Department of Energy's National Oil and Related Programs

by

Dan Maloney, Kevin Doggett, and Liviu Tomutsa
BDM Petroleum Technologies
Under Contract to BDM-Oklahoma, Inc.

September 1997

Work Performed Under Contract No.
DE-AC22-94PC91008

Prepared for
U.S. Department of Energy
National Petroleum Technology Office

NIPER/BDM-0329
September 1997

THREE-PHASE RELATIVE PERMEABILITY CHARACTERISTICS OF A DOLOMITE ROCK PLUG

for

Management and Operating Contract for the Department of Energy's National Oil and Related Programs

Work Performed Under Contract No.
DE-AC22-94PC91008

Prepared for
U.S. Department of Energy
National Petroleum Technology Office

DISCLAIMER

This report was prepared as an account of work sponsored by an agency of the United States Government. Neither the United States Government nor any agency thereof, nor any of their employees, makes any warranty, expressed or implied, or assumes any legal liability or responsibility for the accuracy, completeness, or usefulness of any information, apparatus, product, or process disclosed, or represents that its use would not infringe privately owned rights. Reference herein to any specific commercial product, process, or service by trade name, trademark, manufacturer, or otherwise does not necessarily constitute or imply its endorsement, recommendation, or favoring by the United States Government or any agency thereof. The views and opinions of authors expressed herein do not necessarily state or reflect those of the United States Government or any agency thereof.

BDM-Oklahoma, Inc.
P.O. Box 2565
Bartlesville, Oklahoma 74005

Table of Contents

1.0 INTRODUCTION **1**

2.0 PROJECT DESCRIPTION **1**

2.1 Two-Phase Relative Permeability Results 2

2.2 Three Phase Relative Permeability Results 7

3.0 DISCUSSION **8**

4.0 CONCLUSIONS **9**

APPENDIX **11**

Tables

1 Steady-State Imbibition Relative Permeability Results 3

2 Steady-State Second Drainage Relative Permeability Results 3

3 Oil/Gas Relative Permeability Results at Residual Water 6

4 Water/Gas Relative Permeability Results at Residual Oil 6

5 Drainage Relative Permeability Results at Residual Gas 7

6 Three-Phase Relative Permeability Results at Water 8

7 Three-Phase Relative Permeability Results at Water 8

Figures

1 Steady-State Oil/Water Relative Permeability Results 4

2 Steady-State Oil Relative Permeability Results 4

3 Steady-State Water Relative Permeability Results 5

4 Steady-State Gas Relative Permeability Results 5
5 Fluid Saturation Histories 7

ABSTRACT

Reservoir simulation is an effective tool for predicting production from petroleum reservoirs under various reservoir management schemes. Fluid transmission and retention characteristics of reservoir rock units are necessary for simulation. Although direct measurements of relative permeability and capillary pressure are performed in the laboratory in samples containing only two fluids, i.e., brine-oil, brine-gas, or oil-gas, in petroleum reservoirs the three phases are present. Therefore, it is important to measure relative permeabilities in the presence of the three phases. Because of experimental difficulties in measuring saturations in the three-phase experiments, few accurate experimental data are available in the literature, and there is a strong interest in the industry in accurate and affordable three-phase measurements. Such data are necessary to build accurate models to be used in field simulations.

During this reporting period, experimental procedures—including refinement of in-situ saturation measurements using X-ray and application of syringe pumps for accurate measurement of gas injection volumes—were perfected to allow the accurate measurement of three-phase relative permeability. Actual measurements were performed on a sample from a formation of interest to industry.

ACKNOWLEDGMENTS

This work was performed for the U.S. Department of Energy under contract DE-AC22-94PC91008. The authors thank Min Tham, BDM-Oklahoma, Inc., and Steve George, Leon Grossman, Willis Waldorf, and Ron Masias, BDM Petroleum Technologies, for their assistance in project activities. Appreciation is also expressed to DOE Project Manager Bob Lemmon for his support.

1.0 INTRODUCTION

Multiphase flow is a common phenomenon in production from petroleum reservoirs. The initial or primary production from a reservoir may include gas, oil, brine, or combinations of the three. Later in the productive life of a reservoir, two-phase flow occurs as fluid, such as brine, is injected into a reservoir to boost production. Finally, if improved oil recovery techniques are used to maximize hydrocarbon recovery, multiphase flow processes are virtually guaranteed to occur. With multiphase flow, the fluids compete for the same flow paths through the reservoir rock. The additional resistance to flow is described by normalizing permeabilities for each of the flowing phases at each fluid saturation condition with respect to a base permeability. This measurement and normalization process yields relative permeability data.

The concept of relative permeability for two-phase flow is not new. Work on developing two-phase flow relationships probably began in 1859. Through the years, techniques for using the results have been refined for estimating petroleum reservoir productivity and performance. Efforts to extend the techniques for three-phase flow began in 1941, but difficulties limited progress in this area. Three-phase flow experiments for determining relative permeability relationships are very difficult to perform. Measuring fluid saturations in a rock during three-phase steady-state flow experiments was virtually impossible until the recent advent of techniques to monitor in-situ fluid saturations directly during flow experiments. Correlations have been developed to predict three-phase flow effects from two-phase flow measurements, but such correlations are not always correct or accurate. The primary reasons for the limited knowledge with respect to three-phase flow systems are the scarcity of accurate three-phase relative permeability laboratory data and laboratory measurement systems.

The objective of this work is to address needs in developing and confirming three-phase relative permeability correlations. Knowledge gained from this project is expected to provide guidance on what types of tests are really necessary for three-phase simulation, and how testing times and costs can be minimized while maximizing the usefulness of the data.

2.0 PROJECT DESCRIPTION

Systematic, accurate, three-phase relative permeabilities measurements were performed on a carbonate sample from a Red River formation in the Williston Basin. The Williston Basin is a broad, roughly circular, indistinctly bounded, shallow depression on the southeastern side of the Canadian Shield. At the basin center, Lower Paleozoic rocks attain a maximum thickness in excess of 3,000 ft and are overlain by 12,000 ft of Upper Paleozoic, Mesozoic, and Tertiary strata. The Ordovician Red River Formation was deposited within the basin as several alternating sequences of limestone, dolomite, and anhydrite in subtidal, intertidal, and supratidal environments.

The Red River C interval is commonly subdivided into an upper laminated dolomite and a lower burrowed dolomite porosity zone. Both dolomite porosity zones are productive, with the burrowed porosity zone the major producer. The laminated interval is overlain by a 20-ft anhydrite interval that acts as the seal for the reservoir. Rapid, lateral variations in porosity and permeability, attributed to patterns of dolomitization, occur throughout the C member. Highly localized pods of dolomite beneath the C anhydrite were formed by downward migration of magnesium-rich brines. The pods consist of concentric lenses of tight anhydritic dolomite and fine- to medium-grained porous dolomite, and interfinger laterally with relatively tight limestone. The crests of structures are typically tight with the best porosity developed on the flanks. Irregularly distributed dolomite reservoirs are identifiable by 3D seismic and close well spacing.

Understanding complex variations in rock properties is important to improve reservoir characterization and oil recovery. Core data provide information on various depositional and diagenetic controls that include the pore size and distribution, pore throat size, grain or crystal size, and fluid saturation within the pores. Variations in pore attributes define distinctive zones with similar fluid flow characteristics. The major controls on these features are the sediment source, and the subsequent diagenetic processes of compaction, dissolution, and cementation. Fluid analyses and relative permeability results are necessary for reservoir simulation of fluid movement to determine applicable improved recovery processes.

Steady-state two- and three-phase relative permeability measurements were performed on a Red River core plug from the burrowed dolomite porosity interval from 12,456.1 ft depth to determine relative fluid movement through the pores under different fluid saturations.

2.1 TWO-PHASE RELATIVE PERMEABILITY RESULTS

The experimental techniques developed for three-phase relative permeability measurements are described in the Appendix. Oil and brine fluids were doped or tagged with X-ray absorbing chemicals to allow in-situ fluid saturations to be determined by X-ray absorption techniques.

The permeability to tagged brine was measured to be 8.81 md. More than 20 pore volumes of oil were flowed at rates up to 120 ml/hr (40 ft/day) to reach a residual brine saturation of 0.219. An oil permeability of 8.96 md was measured at this condition. Imbibition and second drainage cycle oil and brine relative permeabilities were measured at seven brine fractional flows ranging from 0.02 to 0.98. Total injection rates (oil plus brine) of 60 ml/hr (20 ft/day) were used during the two-phase measurements. Multiple rates up to 60 ml/hr were used to measure a permeability to brine of 3.56 md at a residual oil saturation of 0.300 after the imbibition cycle, and a permeability to oil of 8.28 md at a residual brine saturation of 0.173 after the second drainage cycle. Relative permeability results are shown in Tables 1 and 2 and Figures 1, 2, 3, and 4. Values have been normalized with respect to the absolute brine permeability of 8.81 md.

The fluids used were prepared according to the following procedures:

- Brine—80 g CsCl + 50 g KCl dissolved in one liter of water
- Oil—200 g bromodecane dissolved in one liter of Soltrol

The viscosities of brine and oil were 1.03 cp and 1.56 cp, respectively. The densities of brine and oil were 1.0871 g/cm^3 and 0.8009 g/cm^3, respectively. For three-phase work, the X-ray filter used consisted of a cuvette filled with a solution prepared by dissolving 20 g CsCl in 50 ml water.

Table 1 Steady-State Imbibition Relative Permeability Results

f_w, fraction	$S_{w,ave}$, fraction	k_{rw}, fraction	k_{ro}, fraction
0.00	0.219	0.00e+00	1.02e+00
0.02	0.305	7.68e-03	5.70e-01
0.05	0.363	1.35e-02	3.89e-01
0.20	0.429	3.38e-02	2.05e-01
0.50	0.491	7.66e-02	1.16e-01
0.80	0.547	1.31e-01	4.95e-02
0.95	0.604	2.31e-01	1.84e-02
0.98	0.639	2.93e-01	9.06e-03
1.00	0.700	4.04e-01	0.00e+00

Table 2 Steady-State Second Drainage Relative Permeability Results

f_w, fraction	$S_{w,ave}$, fraction	k_{rw}, fraction	k_{ro}, fraction
0.98	0.634	2.86e-01	8.83e-03
0.95	0.624	2.47e-01	1.97e-02
0.80	0.553	1.63e-01	6.17e-02
0.50	0.509	7.07e-02	1.07e-01
0.20	0.497	2.91e-02	1.76e-01
0.05	0.369	1.18e-02	3.38e-01
0.02	0.319	6.67e-03	4.95e-01
0.00	0.173	0.00e+00	9.40e-01

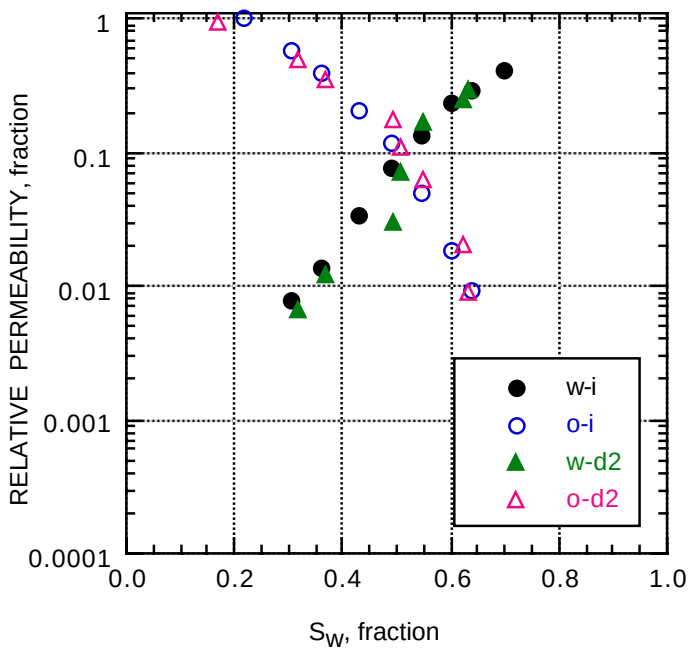

Figure 1 **Steady-State Oil/Water Relative Permeability Results**

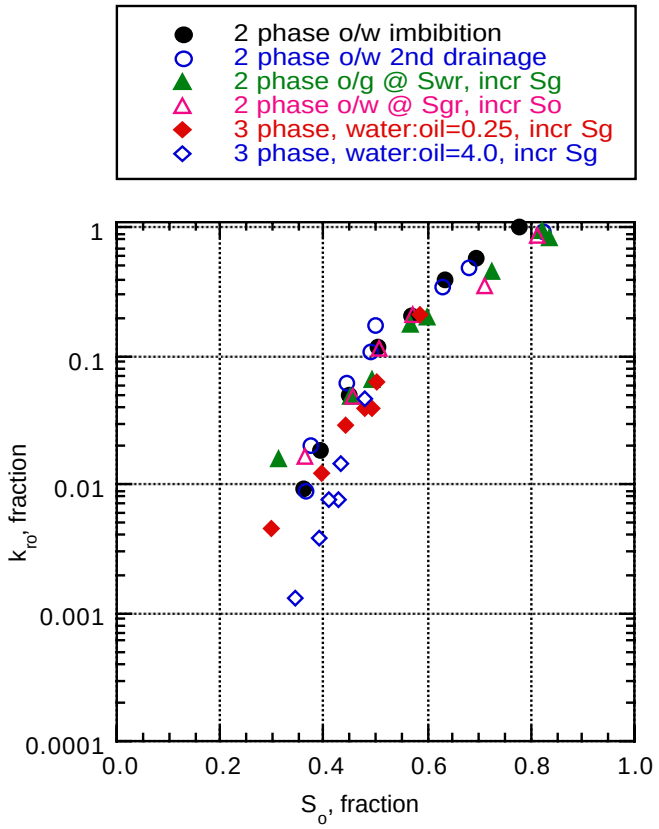

Figure 2 **Steady-State Oil Relative Permeability Results**

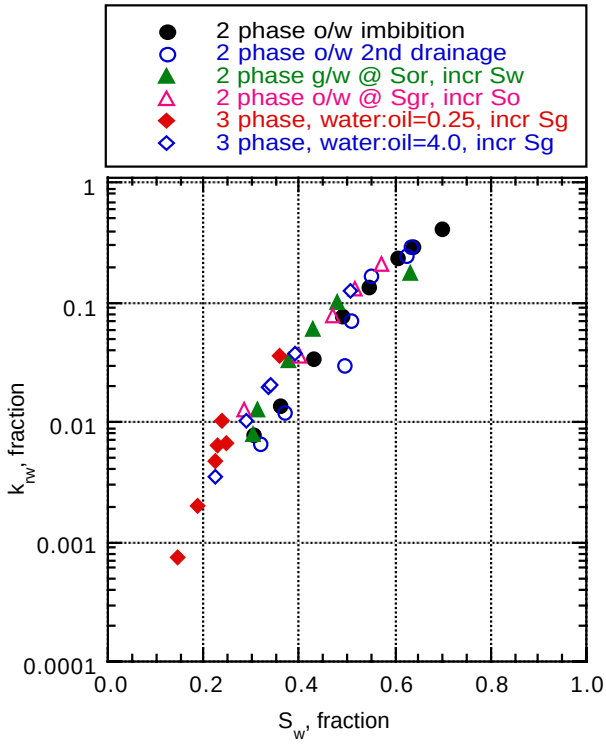

Figure 3 **Steady-State Water Relative Permeability Results**

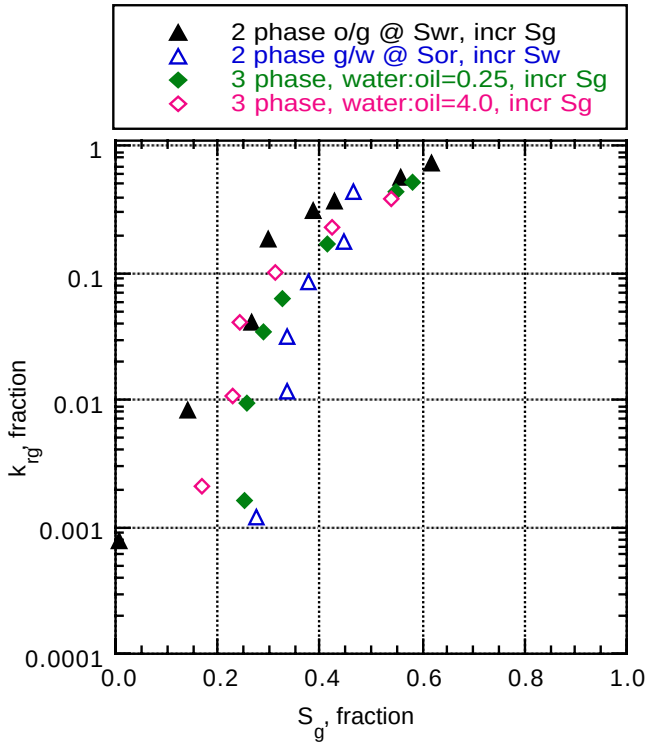

Figure 4 **Steady-State Gas Relative Permeability Results**

A two-phase gas/oil relative permeability test was performed at a residual water condition following the two-phase oil/water second drainage cycle. Nitrogen gas was bubbled through a transfer cylinder containing the test brine and oil before entering the sample. Oil and gas relative permeabilities were measured at gas to liquid ratios ranging from 0 to 3,000. Note that additional water was purged from the core during this cycle. A permeability to gas of 6.33 md was measured after the oil/gas cycle at a residual oil saturation of 0.260 and residual brine saturation of 0.119. The results are shown in Table 3 and Figures 2, 3, and 4. Values have been normalized with respect to the absolute brine permeability of 8.81 md.

Table 3 Oil/Gas Relative Permeability Results at Residual Water

Gas:Oil	$S_{o,ave}$	$S_{w,ave}$	$S_{g,ave}$	k_{ro}	k_{rw}	k_{rg}
0.0	0.827	0.173	0.000	9.40e-01	NA	0.00e+00
0.1	0.840	0.150	0.010	8.27e-01	NA	7.75e-04
1.6	0.727	0.130	0.143	4.48e-01	NA	8.26e-03
17.9	0.601	0.132	0.267	1.94e-01	NA	3.93e-02
89.0	0.571	0.127	0.302	1.76e-01	NA	1.78e-01
421.3	0.495	0.118	0.387	6.41e-02	NA	3.05e-01
663.5	0.456	0.113	0.431	4.78e-02	NA	3.59e-01
3179.7	0.316	0.126	0.558	1.52e-02	NA	5.46e-01
All Gas	0.260	0.119	0.621	0.00e+00	NA	7.19e-01

A two-phase gas/water relative permeability test was performed at a residual oil condition following the two-phase gas/oil cycle. Water and gas relative permeabilities were measured at gas to liquid ratios ranging from 3,000 to 0. Following this cycle, a brine permeability of 1.50 md was measured at a residual oil saturation of 0.241 and residual gas saturation of 0.127. The results are shown in Table 4 and Figures 2, 3, and 4.

Table 4 Water/Gas Relative Permeability Results at Residual Oil

Gas:Water	$S_{o,ave}$	$S_{w,ave}$	$S_{g,ave}$	k_{ro}	k_{rw}	k_{rg}
3228.4	0.227	0.305	0.468	NA	7.70e-03	4.25e-01
815.7	0.235	0.316	0.449	NA	1.23e-02	1.71e-01
152.1	0.244	0.377	0.379	NA	3.25e-02	8.45e-02
30.2	0.234	0.428	0.338	NA	5.97e-02	3.08e-02
11.3	0.233	0.430	0.338	NA	6.00e-02	1.16e-02
0.7	0.237	0.483	0.280	NA	9.71e-02	1.15e-03
0.0	0.240	0.633	0.127	NA	1.70e-01	0.00e+00

A two-phase oil/water relative permeability test was performed at a residual gas condition following the two-phase water/gas test. Oil and water relative permeabilities were measured at brine fractional flows ranging from 0.95 to 0.05. Total injection rates of 60 ml/hr were used

during the measurements. Multiple oil flow rates up to 60 ml/hr were used at the end of this cycle to measure a permeability to oil of 7.57 md at a residual brine saturation of 0.178 and residual gas saturation of 0.007. Note that additional gas was flushed from the sample with increasing oil flow. Results are shown in Table 5 and Figures 2, 3, and 4.

Table 5 Drainage Relative Permeability Results at Residual Gas

f_w, fraction	$S_{o,ave}$	$S_{w,ave}$	$S_{g,ave}$	k_{ro}	k_{rw}	k_{rg}
0.95	0.367	0.576	0.057	1.63e-02	2.06e-01	NA
0.80	0.460	0.518	0.023	4.85e-02	1.29e-01	NA
0.50	0.508	0.470	0.022	1.13e-01	7.50e-02	NA
0.20	0.575	0.405	0.020	2.08e-01	3.45e-02	NA
0.05	0.711	0.287	0.002	3.48e-01	1.23e-02	NA
0.00	0.815	0.178	0.007	8.59e-01	0.00e+00	NA

The two-phase results were used to define a saturation envelope for the sample. The saturation histories are shown in Figure 5.

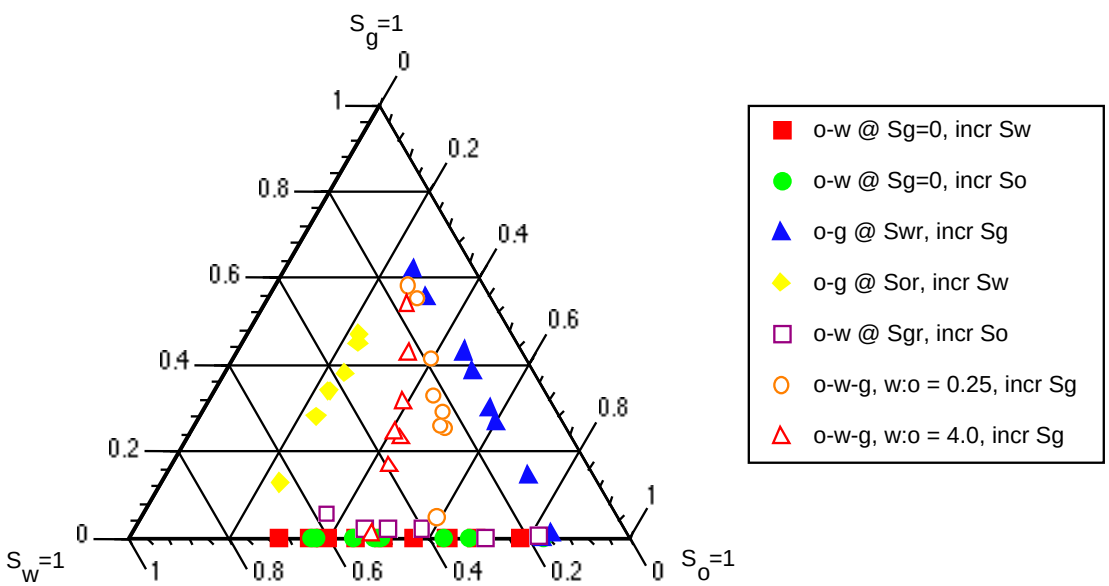

Figure 5 Fluid Saturation Histories

2.2 THREE PHASE RELATIVE PERMEABILITY RESULTS

Following the two-phase oil/water cycle at a residual gas saturation, the sample was allowed to come to equilibrium with two-phase oil/water flow at a brine fractional flow of 0.20 (water:oil = 0.25). A three-phase relative permeability test was then performed by introducing and increasing gas flow while maintaining a water to oil ratio of 0.25. Permeabilities were measured

at gas to liquid ratios ranging from 0 to 7,000. A permeability to gas of 4.49 md was measured after the three-phase test at a residual oil saturation of 0.266 and residual water saturation of 0.152. Results are shown in Table 6 and Figures 2, 3, and 4.

Table 6 Three-Phase Relative Permeability Results at Water:Oil = 0.25

Gas:Liquid	$S_{o,ave}$	$S_{w,ave}$	$S_{g,ave}$	k_{ro}	k_{rw}	k_{rg}
0.0	0.590	0.360	0.050	2.09e-01	3.47e-02	0.00e+00
1.9	0.504	0.241	0.255	6.05e-02	1.00e-02	1.59e-03
16.4	0.493	0.248	0.259	3.91e-02	6.48e-03	9.08e-03
62.4	0.480	0.229	0.291	3.80e-02	6.32e-03	3.35e-02
153.5	0.445	0.226	0.329	2.79e-02	4.64e-03	6.07e-02
994.1	0.396	0.188	0.415	1.19e-02	1.97e-03	1.67e-01
6932.1	0.299	0.149	0.552	4.39e-03	7.29e-04	4.30e-01
All Gas	0.266	0.152	0.583	0.00e+00	0.00e+00	5.10e-01

Following the three-phase test, the sample was flooded with oil to residual water and gas saturations. The sample was allowed to come to equilibrium with two-phase oil/water flow at a brine fractional flow of 0.80 (water:oil = 4.0). A three-phase relative permeability test was then performed by introducing and increasing gas flow while maintaining a water to oil ratio of 4.0. Permeabilities were measured at gas to liquid ratios ranging from 0 to 3,000. A permeability to gas of 3.28 md was measured after the three-phase test at a residual oil saturation of 0.287 and residual water saturation of 0.172. Results are shown in Table 7 and Figures 2, 3, and 4.

Table 7 Three-Phase Relative Permeability Results at Water:Oil = 4.0

Gas:Liquid	$S_{o,ave}$	$S_{w,ave}$	$S_{g,ave}$	k_{ro}	k_{rw}	k_{rg}
0.0	0.482	0.508	0.010	4.63e-02	1.23e-01	0.00e+00
2.6	0.437	0.394	0.169	1.40e-02	3.71e-02	2.09e-03
25.2	0.429	0.338	0.233	7.41e-03	1.96e-02	1.06e-02
94.1	0.410	0.344	0.246	7.50e-03	1.99e-02	3.99e-02
461.6	0.393	0.292	0.315	3.79e-03	1.01e-02	9.91e-02
3039.3	0.346	0.226	0.428	1.30e-03	3.45e-03	2.23e-01
All Gas	0.287	0.172	0.541	0.00e+00	0.00e+00	3.72e-01

The saturation histories for the three-phase measurements are shown in Figure 5.

3.0 DISCUSSION

Relative permeabilities were calculated by normalizing effective permeabilities with respect to the specific permeability of the sample to brine. This normalization process was used to provide consistency with methods of other investigations.

The rock was not cleaned after each two- or three-phase saturation cycle. Although one might anticipate added hysteresis effects from this process, two- and three-phase relative permeabilities a particular fluid phase were primarily affected by the saturation of that phase. Oil and brine relative permeability versus saturation functions exhibited the least hysteresis. Three-phase gas relative permeabilities fell within the hysteresis envelope from two-phase gas results.

Oil relative permeability versus oil saturation trends and brine relative permeability versus brine saturation trends were similar for phase saturations greater than 0.40. Residual oil saturations were similar from both two- and three-phase flow tests. Lower water saturations were attained during three-phase tests compared to two-phase test results. It is suspected that this resulted because the rock has a somewhat greater affinity for oil than for brine.

The manner in which two- and three-phase results were collected, by first defining the outer boundaries of the three-phase saturation envelope and then performing a limited number of trajectories with three flowing phases, worked well. The laboratory staff coined the phrase "walking the dog" to describe this process. The total time required to obtain all the measurements described in this report was less than three months. This measurement sequence appears to offer an economical means of describing two- and three-phase relative permeability functions during a reasonable time frame.

4.0 CONCLUSIONS

Some conclusions from this work on a dolomite rock plug follow:

1. Two- and three-phase relative permeabilities for a particular fluid phase were mostly affected by the saturation of that phase. This was true for gas, oil, and brine relative permeability versus saturation functions.
2. Lower residual brine saturations were achieved during three-phase tests compared to those from two-phase tests. It is suspected that the rock had a slightly greater affinity for oil than for water. Capillary pressure measurements may be performed to confirm this in the future.
3. The manner in which two- and three-phase results were collected, by first defining the boundaries of the three-phase saturation envelope and then performing a limited number of three-flowing-phase saturation trajectories, worked well. This sequence appears to offer benefits of steady-state relative permeabilities versus saturation measurements in a timely, cost-effective manner.

APPENDIX

2D X-RAY SCANNER AND ITS USES IN LABORATORY RESERVOIR CHARACTERIZATION MEASUREMENTS

by Dan Maloney and Kevin Doggett
BDM Petroleum Technologies

Presented at Fourth International Reservoir Characterization Technical Conference, Houston, Texas, March 2–4, 1997

ABSTRACT

X-ray techniques are used in petroleum laboratories for a variety of reservoir characterization measurements. This paper describes the configuration of a 2D X-ray scanner and many of the ways in which it simplifies and improves the accuracy of laboratory measurements.

Linear X-ray scanners are most often used to provide descriptions of fluid saturations within core plugs during flow tests. We configured our linear scanner for both horizontal and vertical movement. Samples can be scanned horizontally, vertically, or according to horizontal and vertical grids. X-ray measurements are fast, allowing measurements of two- and three-phase fluid saturations during both steady- and unsteady-state flow processes. Rock samples can be scanned while they are subjected to stress, pore pressure, and temperature conditions simulating those of a petroleum reservoir.

Many types of measurements are possible by selecting appropriate X-ray power settings, dopes, filters, and collimator configurations. The scanner has been used for a variety of applications besides fluid saturation measurements. It is useful for measuring porosity distributions in rocks, concentrations of X-ray dopes within flow streams during tracer tests, gap widths in fracture flow cells, fluid interface levels in PVT cells and fluid separators, and other features and phenomena.

HARDWARE

Many researchers have used X-rays to determine two- and three-phase fluid saturations in rocks.[1-11] The system used by the authors is based primarily on systems described by Oak, Potter, and others,[7-11] except that scans can be taken in both horizontal and vertical directions. Figure 1 is a general schematic of the X-ray scanner used by BDM Petroleum Technologies.[12,13] The figure shows the relative position of a sample with respect to the X-ray source and detector.

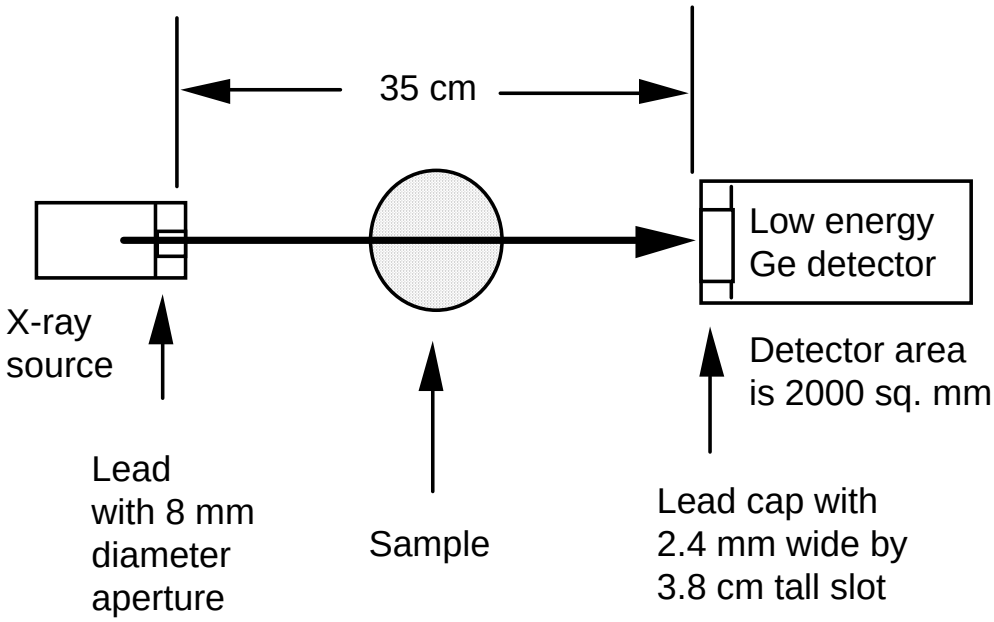

Figure 1 General Schematic of the X-Ray Source and Detector

The X-ray source is a Phillips PW2184/00 tungsten target XRF tube. The tube is rated for 3 kW at 100 kV, although normal operating conditions include voltages from 25 to 60 kVp and currents to 80 mA. The tube is normally operated with peak voltages close to but above the k-emission energies of X-ray dopes contained in test fluids. This yields maximum contrast between X-ray absorption characteristics of the test fluids. The tube is powered by a Phillips XRG 3100 X-ray generator.

The portion of the tube that emits X-rays is housed within a thick, lead-lined stainless steel turret that has several collimation ports of different lengths. A lead shutter within the turret is normally closed unless a scan is taking place. The ends of the collimation ports are machined to accept cuvettes containing doped fluid solutions for beam conditioning.

A chiller is required to protect the tube from heat damage. The chiller used with this X-ray device was made by the Haskris Co.

The X-ray detector is a Canberra low energy germanium detector, which has a 2,000 sq. mm area, 20 mm thickness, 0.5 mm Beryllium window, and the following resolution characteristics: FWHM at 5.9 keV of 400 eV and FWHM at 122 keV of 700 eV. The detector has an RC preamplifier. The detector electronics are cooled by liquid nitrogen using a 15-liter, horizontal integral cryostat. The 15-liter capacity provides about 10 days of operation before the cryostat must be refilled with liquid nitrogen. To prevent damage to the detector from a low liquid nitrogen condition, the preamplifier has a high-temperature inhibitor. Damage can also occur if full power is suddenly applied to the deenergized detector. To protect against this occurrence,

power to the detector passes through a pull-down switch that protects against sudden off-and-on power cycles during storms. An integrated signal processor, slave board, and software are used for multichannel data acquisition and analysis. These reside within a Gateway 486 computer.

The detector is surrounded by a lead shield. A thick lead cap was installed into the end of the detector shield between the detector and sample. The lead cap contains a slit that limits X-rays that reach the detector to only those which pass through the test sample. The slit is used to gain better resolution of position-specific X-ray intensities during linear X-ray scans. For scans on horizontal samples, the slit is positioned vertically. For scans on vertical samples, the slit is positioned horizontally. For samples in which X-ray scans are taken in two dimensions (vertical and horizontal), another lead cover with a 2 mm aperture is placed in front of the detector.

The X-ray tube and detector are mounted on an inverted U-shaped frame. The horizontal and vertical positions of this frame are controlled by drive screws and motors. Parker Compumotor indexers and motors along with other hardware are used to control the horizontal and vertical movement of the scanning platform. The Compumotor indexers controlling the horizontal and vertical stages of the X-ray scanner are daisy-chained so that commands to change the scanner horizontal and vertical positions are sent through a single communication channel. The laboratory PC computer communicates with the indexers during X-ray scans. As a sample is scanned, the X-ray tube and detector move with respect to the stationary samples.

As previously stated, the laboratory computer is used for data acquisition and X-ray scanner control. The system uses LabVIEW, a software product by National Instruments, for these functions. The computer also controls pumps and other laboratory hardware, collects data from instruments, and performs calculations using measured data.

GENERAL X-RAY SCANNER OPERATION

Samples to be scanned are mounted within the scanning region of the X-ray device. The horizontal scan range is approximately 3 meters while the vertical scan range is approximately 0.6 m. An X-ray scan consists of a number of X-ray intensity measurements taken at discrete positions along the length and height of a sample. For small rock samples, scan increments of 0.1 to 0.5 cm are often employed. A scanning pattern is determined for a sample during the initial stages of experimentation. Scan parameters are entered into the computer program. Thereafter, scans can be automatically programmed for specific time intervals.

When a scan is initiated, the X-ray device moves to the first measurement position. Upon reaching the first position, the scanner stops moving. The lead shutter opens, emitting X-rays. The intensities of X-rays that pass through the sample are measured by the detector. After the predefined count interval, which is usually about five seconds, the X-ray device moves to the next position. Intensities are measured at the second position, then the scanner moves again.

This process continues until measurements have been recorded at each scan position. Upon completing the final measurement, the lead shutter closes. Scanning an 8-cm-long sample at 15 positions takes about two minutes. Faster scans are also possible, making the device useful for determining changing saturations during unsteady-state tests.

The first sets of X-ray scans taken of a sample are used to correlate X-ray intensities to fluid contents or in-situ rock fluid saturations. Once these correlations are established, they are entered into the scanning program. For subsequent scans, the correlation equations are used to calculate fluid saturations as soon as X-ray intensities are measured. Results are plotted on the computer's screen, providing a real-time image of the saturation conditions within the sample.

Several experiments on different samples are often conducted at the same time. The only restriction here is that scan times have to be scheduled in a manner that avoids conflicts.

X-Ray Terminology and Basic Calculations

X-ray measurements described in the following sections of this report are for various X-ray tube voltage and current settings. Because the X-ray source is polychromatic, X-rays with a range of photon energies are emitted from the X-ray tube for particular X-ray generator settings. For this reason, the X-rays which pass through the sample and reach the detector also are over a range of photon energies.

Figure 2 shows intensities of X-ray photons that passed through a coreholder for various tube voltage and current settings.[12] A fairly broad band of X-rays pass through a sample during a typical X-ray scan. For example, for scans of Figure 2 with the X-ray generator set to 55 kV, intense X-rays were within a range from about 40 keV to 60 keV with greatest intensity at around 55 keV. Increasing the tube voltage shifts the region of greatest intensity to a higher photon energy and increases the relative intensities of the photons which emerge from the coreholder. Increasing the tube current while keeping the voltage constant generally increases the amplitude of the photon intensity distribution plot. Another way to increase intensities at the detector is to increase the area of the collimator, allowing greater numbers of photons to reach the detector. Decreasing the collimator area decreases the intensities of detected photons, but provides a better measure of the photons which pass through a specific region of the sample.

The X-ray detector is used to count the number of photons which emerge from the coreholder over a specified live-time interval (part of the total detector time is dead-time). Intensities are calculated by dividing the number of counts by the live-time interval in seconds.

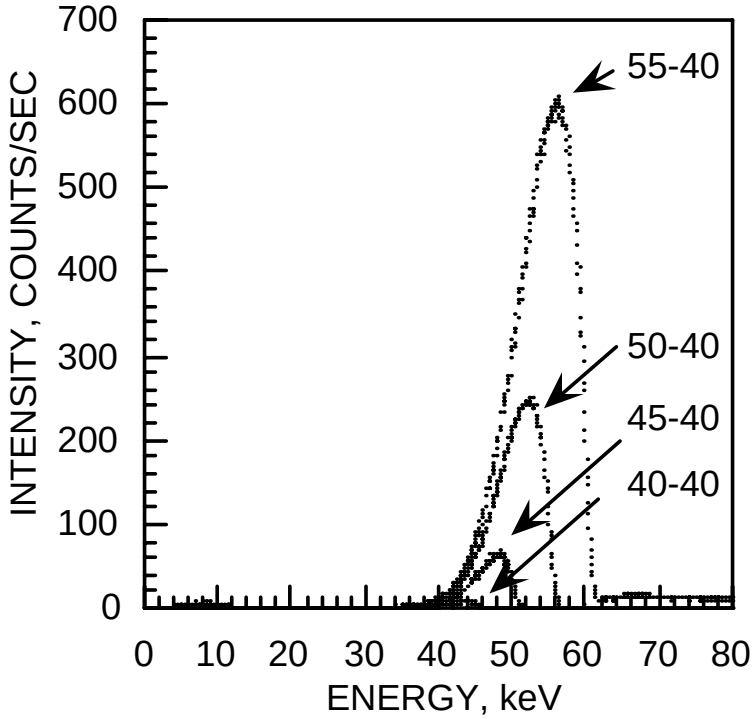

Figure 2 **X-Ray Results from Scans through an Aluminum Coreholder of a Bluejacket Sandstone Plug . X-ray generator kV and mA settings (kV-mA) are shown from scans with different tube voltages.**

Lambert's Law is often cited[14,15] to relate intensities of X-rays which emerge from a sample to intensities of X-rays which are incident to the sample:

$$I = I_o e^{(-kx)} \quad (1)$$

where I is the emergent intensity, I_o is the incident intensity, k is the linear absorption coefficient of the sample, and x is the sample thickness. Taking natural logs of both sides of Equation 1 and manipulating the result yields:

$$Ln(I) = -kx + Ln(I_o) \quad (2)$$

When more than one absorber is in the X-ray beam path, the equation is:

$$I = I_o e^{(-k_1 x_1 - k_2 x_2 - \ldots)} \quad (3)$$

For typical rock fluid saturation measurements, I_O, the X-ray absorption characteristics of the specific rock and coreholder assembly, and the X-ray path length are constants so that changes in Ln(I) result from changes in rock fluid saturations. As long as incident X-ray intensities remain constant throughout a particular flow experiment in which X-ray absorption techniques are used for fluid saturation measurements, a value for the incident intensity is not specifically required. However, knowledge of incident X-ray intensities is important when predicting X-ray absorption characteristics of experimental fixtures that have never been scanned before. X-ray scan results from this laboratory are usually described using natural logs of emergent X-ray intensities because this is the variable predominantly used for rock fluid saturation calculations.

X-Ray Calibrations

For tests in which two different fluids exist within the sample, one of the fluids is typically doped with an X-ray absorber, such as sodium iodide in the brine phase or bromodecane in the oil phase.

Figure 3 shows X-ray data from scans of a particular position within a rock sample when the rock was completely saturated with air, then oil, and finally with a doped brine.[16] The absorption characteristics of the sample change significantly with changes in fluid content. Figure 4 shows the result of taking the natural log of the integrated intensities under each curve to construct two-phase saturation calibrations. The figure shows correlations for air-brine and oil-brine fluid systems. Using these types of calibrations for each scan position within the rock, two-phase fluid saturations within rock samples can be easily determined from X-ray measurements. Figure 5 shows a typical result from a coreflood experiment. The saturation gradient toward the outlet end of the sample is probably indicative of a capillary end-effect.

For tests with three fluid phases, two of the fluids are doped with absorbers that have X-ray absorption edges at different energies. Additionally, the incident X-ray beam is filtered by passing it through an absorber that splits the distribution of intensities into two distinct regions. Figure 6 provides an example in which containers filled with water, water doped with potassium bromide, and water doped with sodium iodide were scanned using a filtered X-ray beam.[16] As shown, the dopes yield different absorption characteristics for each fluid on each side of the split. Figures 7 and 8 show how taking the natural log of the integrated intensities under each curve provide sets of equations that can be used to determine three-phase saturations from a single X-ray scan. Figure 9 graphically shows how these results are used to calculate three-phase saturations. The beauty of this "dual energy" technique is that saturations for each of the three fluid phases are calculated from data measured during a single X-ray scan.

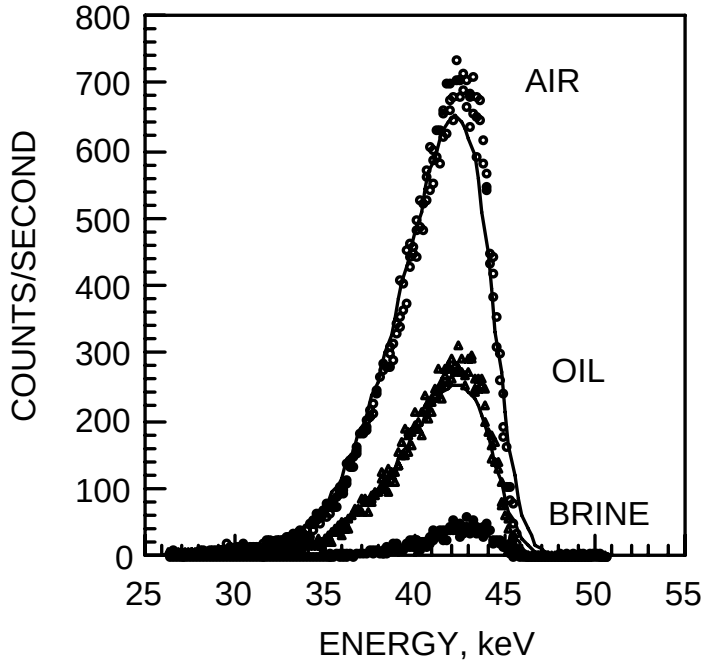

Figure 3 **X-ray Scan Data for One Scan Position with Different Saturating**

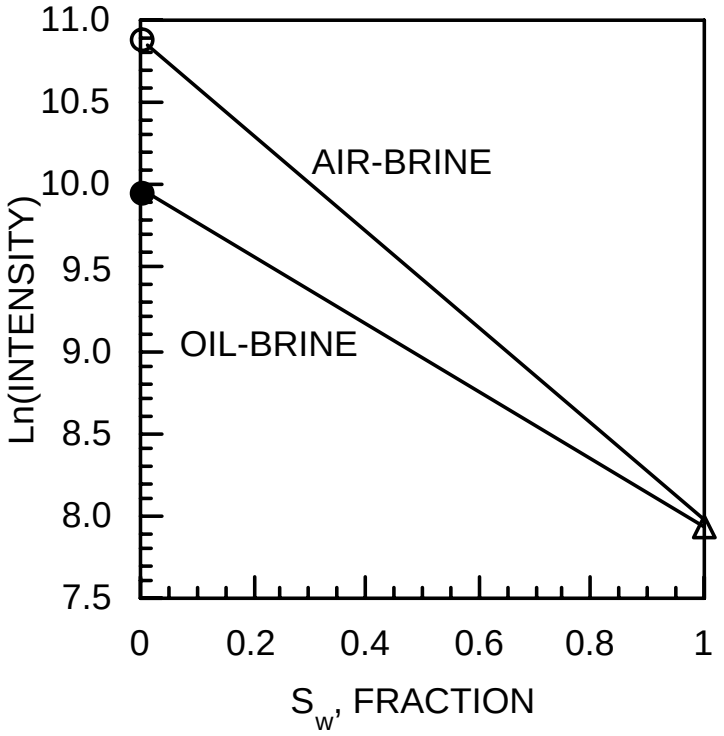

Figure 4 **Resulting X-Ray Correlations to Fluid Saturations**

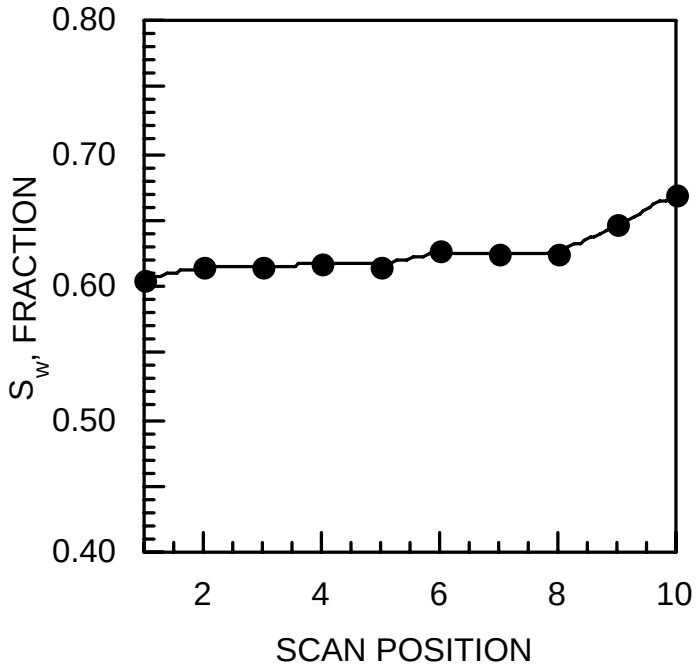

Figure 5 **Typical Scan Results Showing an End-Effect**

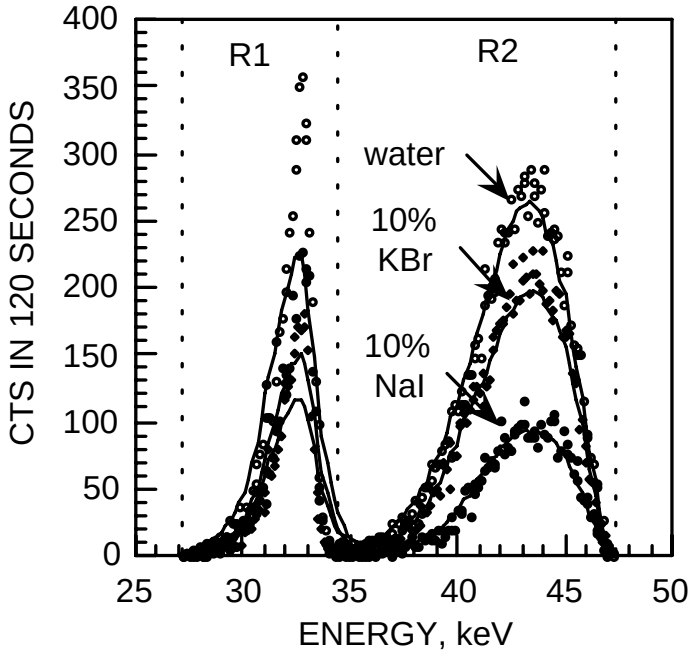

Figure 6 **Intensities from "Dual Energy" Measurements**

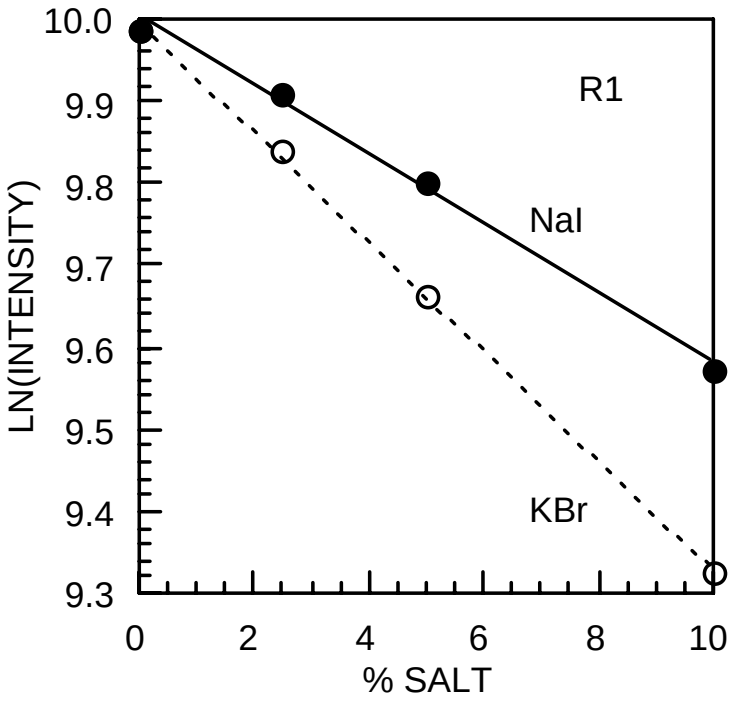

Figure 7 **Resulting X-Ray Range 1 Correlations to Saturations**

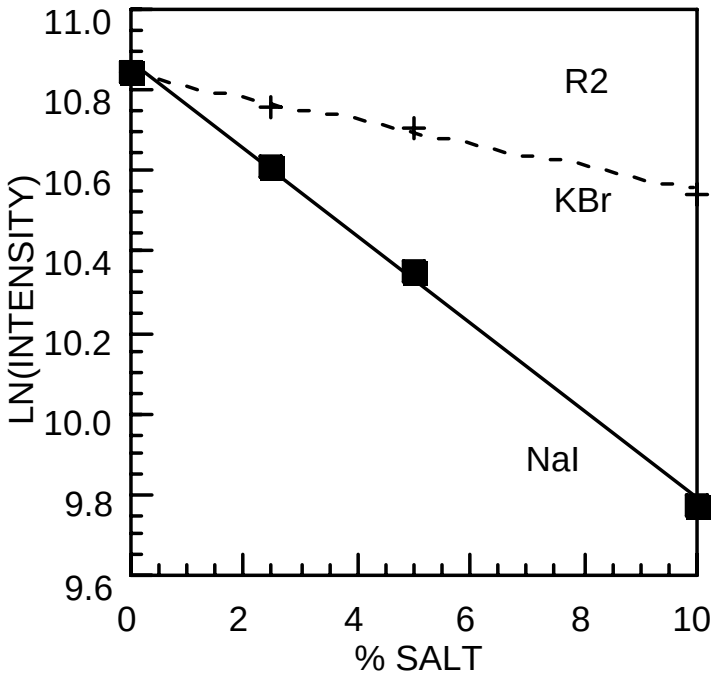

Figure 8 **Resulting X-Ray Range 2 Correlations to Saturations**

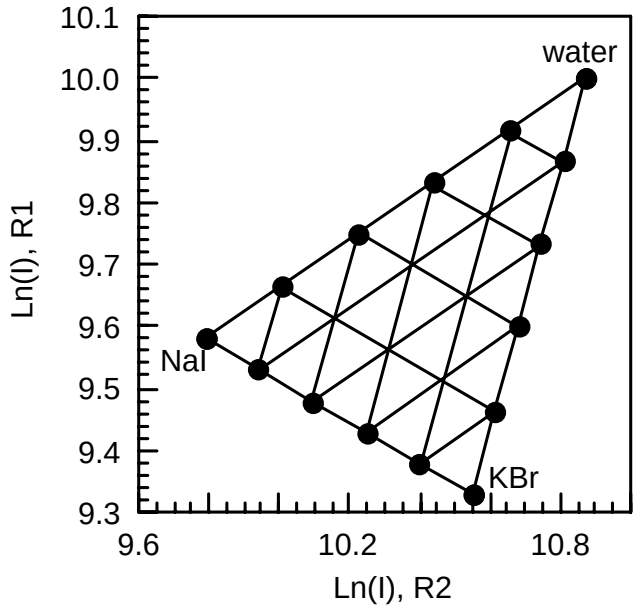

Figure 9 **Determination of Three-Phase Saturations from Range 1 and Range 2 X-Ray Measurements**

X-RAY SCANNER APPLICATIONS

The following lists some of the more novel measurements that have been performed using the scanner.

Corefloods

The X-ray scanner is commonly used for two and three-phase steady- and unsteady-state relative permeability tests and corefloods. Figure 10 shows a simple schematic of a closed-loop flow system that was used for three-phase measurements during a reservoir condition coreflood. Rock fluid saturations were determined by X-ray scanning the core plug through the coreholder. Produced fluid volumes were determined by vertically scanning the fluid separator.

As shown by Figure 11, fluid interface levels within the separator are easily determined from X-ray results. The interface levels can be clearly defined from step-changes in X-ray intensities. The X-ray technique for measuring fluid volumes within a separator is effective even when the fluids mix or form emulsions. Scans of fluids within the separator can be used to determine linear X-ray absorption coefficients for the fluids "on the fly" so that X-ray calibrations can be adjusted for changes in fluid properties.[16] This type of X-ray technique is also applicable for PVT measurements and provides an added advantage in that windowless cells can be employed.

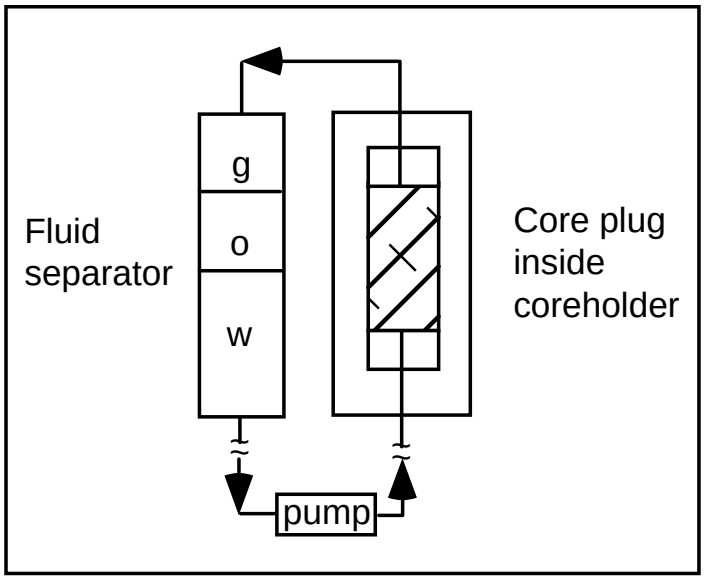

Figure 10 Simple Schematic of Closed-Loop Flow System

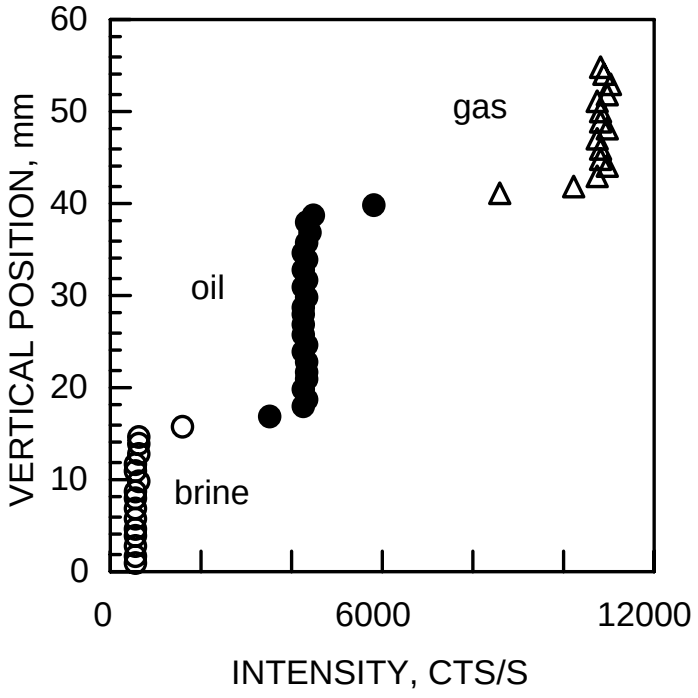

Figure 11 Fluid Interface Level Measurements from Separator Scan

Porosity Distribution Imaging

Rock porosity distributions can be calculated from X-ray intensity measurements.[9] Software can be used to create images from the 2D X-ray data. Figure 12 shows results for a 10 x 10 x 3 cm sandstone block.[17] The block was X-ray scanned while dry and then after it was saturated with brine. Intensity measurements were recorded at about 1,000 horizontal and vertical positions. Differences in X-ray intensities for the dry and brine saturated sample and the total porosity were used to calculate porosity distributions. Permeabilities measured along the lower face of the dry sample by a probe permeameter are overlaid on the porosity map. This information simplified interpretations of results from subsequent spontaneous imbibition measurements.[17]

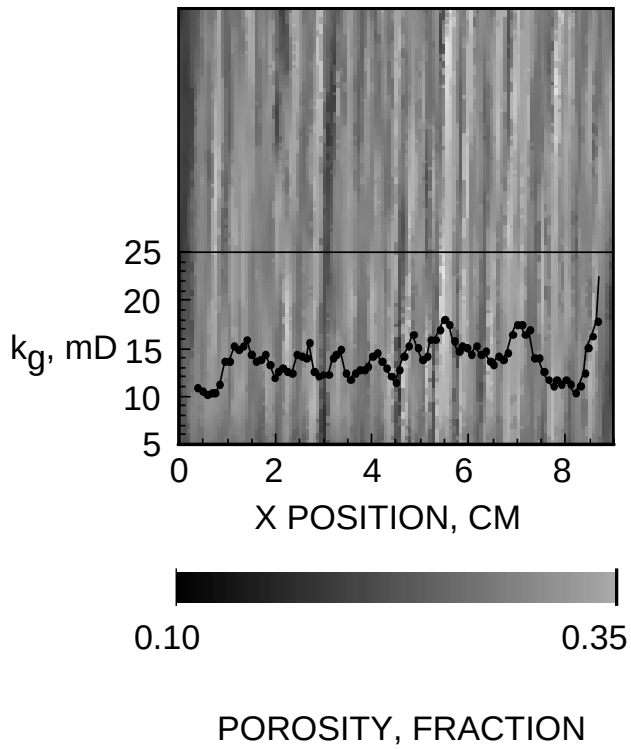

Figure 12 **Characteristics of a Berea Sandstone Slab. Porosities were calculated from X-ray measurements of the dry and brine-saturated rock. Permeabilities were from probe minipermeameter measurements.**

Determination of Fluid Saturations within Fracture Models

X-rays techniques are also particularly well suited for measurements of fluid flow properties in fractures or cracks. Figure 13 is a schematic of a plastic fracture model that was used for multiphase fluid flow measurements in fractures.[17,18] The fracture gap width within the cell was 790 μm. Flow properties and saturation distributions were measured as oil and brine flowed upward through the cell.

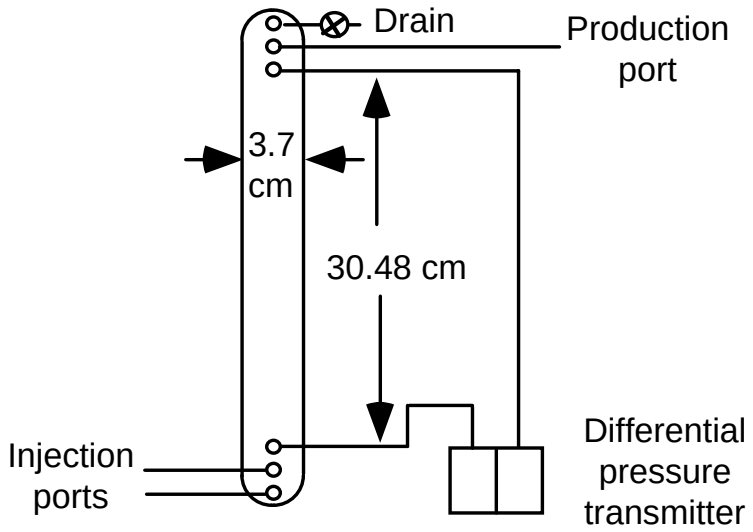

Figure 13 Simple Fracture Cell Schematic

In addition to measurements of fluid saturations, the X-ray device was also found to be an effective tool for measuring the width of the open fracture. Fracture widths were measured with resolution to about 5 μm.

Figure 14 shows saturation profiles that were measured by the X-ray scanner during this steady-state relative permeability test. For each steady-state flow condition in this particular test, the oil flowed through a narrow stream in the center of the fracture. Contrary to what some might expect, the brine saturation was considerably different from the brine fractional flow.

Figures 15 and 16 provide comparisons of fracture relative permeabilities for two different fracture widths with vertical upward flow. As shown, relative permeabilities are considerably different for wide and narrow fractures. Differences in fluid densities and the direction of fluid flow had pronounced effects on results for the wide fracture. As shown by these results, the 2D X-ray scanner was a useful tool for fracture relative permeability measurements. This X-ray application should help to resolve some of the questions concerning multiphase flow in fractures.

Tracer Tests

The X-ray scanner is also useful during tracer tests to evaluate changes in in-situ rock fluid saturations as well as tracer concentrations in the effluent. With the X-ray generator set at its lowest tube power settings of 25 kV and 1 mA, X-ray scans of fluid-filled tubes were used to identify changes in salt concentrations in a brine.[16] Adding salt to the brine increased the X-ray attenuation appreciably, much like what happens when an X-ray absorber is added to a test fluid with higher tube power settings. This application provides flexibility for tracer tests when dopes or other unnatural compounds cannot be added to the rock fluids.

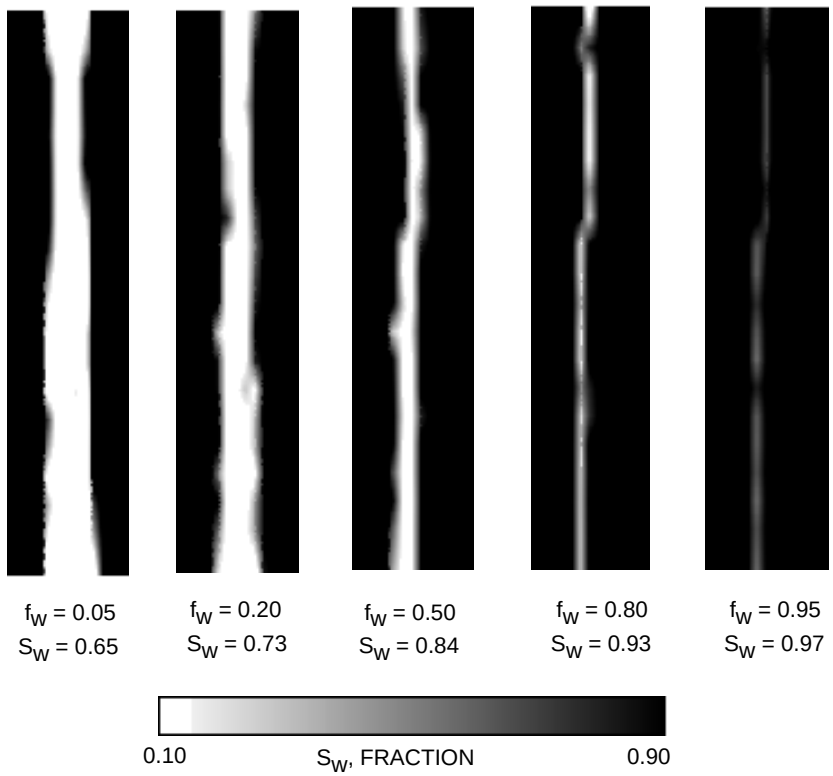

Figure 14 **Two-Phase Oil-Brine Saturation Profiles within a 790 μm Wide Fracture. The flow was vertically upward.**

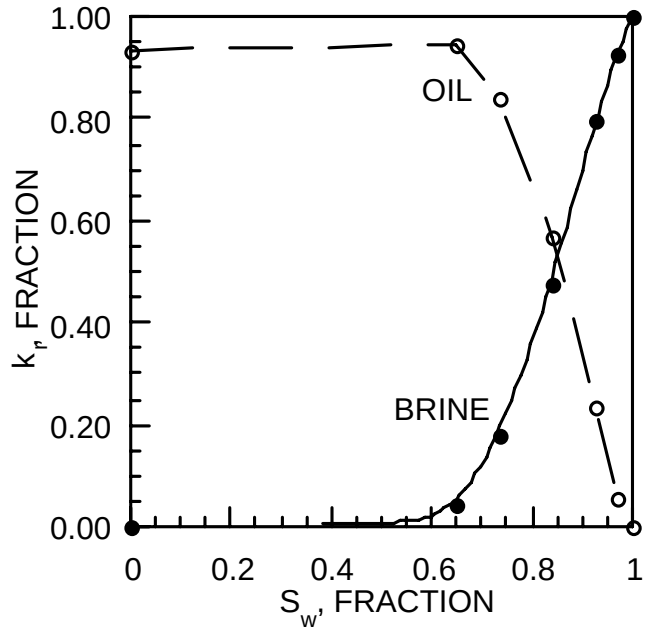

Figure 15 **Oil-brine Relative Permeability Results, 790 μm Fracture. The flow direction was upward.**

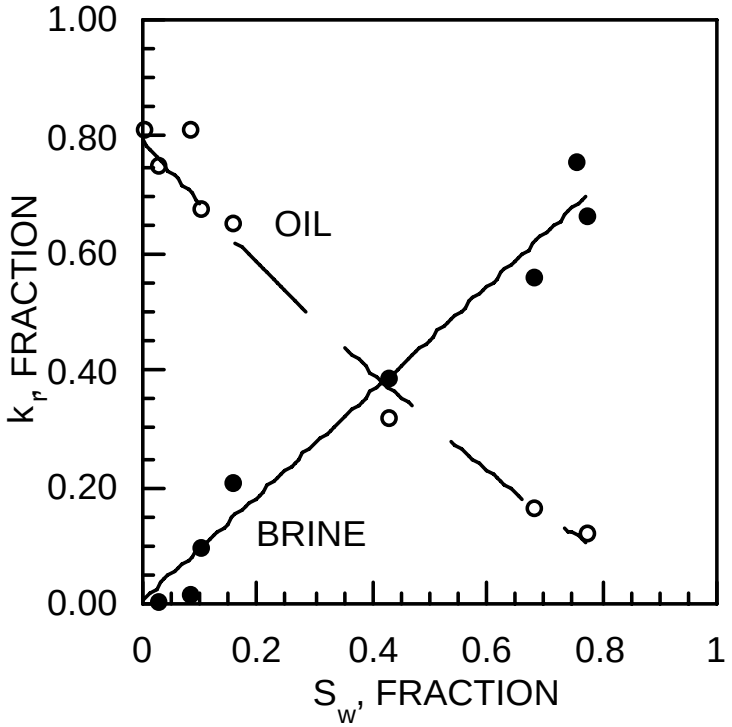

Figure 16 **Oil Brine Relative Permeability Results, 50 μm Fracture. The flow direction was upward.**

CONCLUSIONS

In conclusion, many types of rock and fluid characterization measurements are possible using a 2D X-ray scanning device and appropriate X-ray power settings, dopes, filters, and collimator configurations. While linear scanners have traditionally been used for measuring fluid saturations in rocks, X-ray data from the scanner can also be used to create images of rock and fluid distribution characteristics. The scanner is useful for measuring porosity distributions in rocks, concentrations of X-ray dopes within flow streams during tracer tests, gap widths in fracture flow cells, fluid interface levels in PVT cells and fluid separators, and other features and phenomena. In essence, X-ray scanners are powerful tools for a variety of applications in petroleum laboratories.

ACKNOWLEDGMENTS

The authors express appreciation to U.S. Department of Energy for supporting the preparation and publication of this paper. Many of the X-ray applications reported in this paper were developed during the performance of Department of Energy funded projects. We thank the management of BDM Petroleum Technologies for giving permission to publish this work.

REFERENCES

1. Boyer, R., F. Morgan and M. Muskat: A New Method for Measurement of Oil Saturation in Cores. Trans. AIME, vol. 170, 1947, pp. 15–33.

2. Morgan, F., J. McDowell, and E. Doty: Improvements in the X-ray Saturation Technique of Studying Fluid Flow. Petroleum Transactions, AIME, vol. 189, 1950, pp. 183–194.

3. Laird, A. and J. Putnam: Fluid Saturation in Porous Media by X-ray Technique. Petroleum Transactions, AIME, vol. 192, 1952, pp. 275–284.

4. Laird, A. and J. Putnam: Three Component Saturation in Porous Media by X-Ray Techniques. Petroleum Transactions, AIME, v. 216, 1959, pp. 216–220.

5. Schneider, F. and W. Owens: Sandstone and Carbonate Two- and Three-Phase Relative Permeability Characteristics. Soc. of Petr. Eng. Journal, March 1970, pp. 75–84.

6. Schneider, F. and W. Owens: Steady-State Measurements of Relative Permeability for Polymer/Oil Systems. Soc. of Petr. Eng. Journal, February 1982, pp. 79–86.

7. Oak, M. and R. Ehrlich: A New X-Ray Absorption Method for Measurement of Three-Phase Relative Permeability. Paper SPE 14420 presented at the 60th Annual Technical Conference and Exhibition of the Society of Petroleum Engineers, Las Vegas, NV, September 22–25, 1985.

8. Oak, M., L. Baker, and D. Thomas: Three-Phase Relative Permeability of Berea Sandstone. Paper SPE/DOE 17370 presented at the 1988 SPE/DOE Symposium on Enhanced Oil Recovery, Tulsa, OK, April 17–20.

9. Potter, G. and D. Groves: Displacements, Saturations, and Porosity Profiles from Steady-State Permeability Measurements. Paper SPE 19679 presented at the 64th Annual Technical Conference and Exhibition of the Society of Petroleum Engineers, San Antonio, TX, October 8–11, 1989.

10. Oak, M.: Three-Phase Relative Permeability of Water-Wet Berea. Paper SPE/DOE 20183 presented at the 1990 SPE/DOE Symposium on Enhanced Oil Recovery, Tulsa, OK, April 22–25.

11. Oak, M.: Three-Phase Relative Permeability of Intermediate-Wet Berea Sandstone. Paper SPE 22599 presented at the 66th Annual Technical Conference and Exhibition of the Society of Petroleum Engineers, Dallas, TX, October 6–9, 1991.

12. Maloney, D. and K. Doggett: Advances in Steady- and Unsteady-State Relative Permeability Measurements and Correlations FY 1995. Report NIPER/BDM-0160 prepared under DOE contract DE-AC22-94PC91008, July 1995, pp. 21–28.

13. Maloney, D. and L. Tomutsa: Use of X-Ray Scanners in Petroleum Research. Paper HD 31D-03 presented at the 1995 Fall Meeting of the American Geophysical Union, San Francisco, CA, December 11–15, 1995.

14. Sproull, W.: X-Rays in Practice. McGraw Hill, New York, 1946.

15. Bertin, E.: Principles and Practice of X-ray Spectrometric Analysis. Plenum Press, New York, 1970.

16. Maloney, D. and K. Doggett: Relative Permeability Research FY 1994. Report NIPER/BDM-0067 prepared under DOE contract DE-AC22-94PC91008, September 1994, pp. 23–29.

17. Chang, M. and D. Maloney: Analytical Solutions and Experiments to Two-Phase Flow Problems of Naturally Fractured Reservoirs, Imbibition Transfer Function. Report NIPER/BDM-0171 prepared under DOE contract DE-AC22-94PC91008, September 1995, p. 124.

18. Maloney, D., K. Doggett, and A. Sarkar: Laboratory Characterization of Oil Production Mechanisms in Fractured Rock. Report NIPER/BDM-0274 prepared under DOE Contract DE-AC22-94PC91008, September 1996, pp. 9–21.